In-flight effective area calibration of the *Chandra* low energy transmission grating spectrometer

Deron Pease[1], Jeremy J. Drake[1], Vinay Kashyap[1], Herman L. Marshall[2], Erica L. Raffauf[1], Peter W. Ratzlaff[1], Bradford J. Wargelin[1]

[1]Smithsonian Astrophysical Observatory, 60 Garden Street, Cambridge, MA, USA 02138
[2]Center for Space Research, M.I.T., Cambridge, MA, USA 02139

ABSTRACT

We present the in-flight effective area calibration of the Low Energy Transmission Grating Spectrometer (LETGS), which comprises the High Resolution Camera Spectroscopic readout (HRC-S) and the Low Energy Transmission Grating (LETG) aboard the *Chandra X-ray Observatory*. Previous studies of the LETGS effective area calibration have focused on specific energy regimes: 1) the low-energy calibration for which we compared observations of Sirius B and HZ 43 with pure hydrogen non-LTE white dwarf emission models; and 2) the mid-energy calibration for which we compared observations of the active galactic nuclei PKS 2155−304 and 3C 273 with simple power-law models of their seemingly featureless continua. The residuals of the model comparisons were taken to be true residuals in the HRC-S quantum efficiency (QE) model. Additional in-flight observations of celestial sources with well-understood X-ray spectra have served to verify and fine-tune the calibration. Thus, from these studies we have derived corrections to the HRC-S QE to match the predicted and observed spectra over the full practical energy range of the LETGS. Furthermore, from pre-flight laboratory flatfield data we have constructed an HRC-S quantum efficiency uniformity (QEU) model. Application of the QEU to our semi-empirical in-flight HRC-S QE has resulted in an improved HRC-S on-axis QE. Implementation of the HRC-S QEU with the on-axis QE now allows for the computation of effective area for any reasonable *Chandra*/LETGS pointing.

Keywords: *Chandra*, X-ray, X-ray spectroscopy, transmission grating, calibration

1. INTRODUCTION

The in-flight science instrument calibration of the *Chandra X-ray Observatory* began in August 1999, immediately after launch. The Low Energy Transmission Grating Spectrometer (LETGS) which comprises the High Resolution Camera Spectroscopic readout (HRC-S) and the Low Energy Transmission Grating (LETG; for a description of the LETG and first-light reports see Brinkman et al. 2000a, Brinkman et al. 2000b). The goal of the LETGS calibration effort is to accurately model the LETGS response over its entire active energy range of 0.06−6.0 keV (wavelengths 2−200 Å). Prior to in-flight calibration, the on-axis quantum efficiency (QE) at the nominal aimpoint of the HRC-S was calibrated in the laboratory over the energy range 0.28−10.0 keV (44−1.24 Å). QE calibration for energies < 0.28 keV (λ > 44 Å) was incomplete, as was the HRC-S QE uniformity. The latter is required for computing the LETGS dispersed effective area, which physically covers three microchannel plates (MCPs) and spectrally covers more than two orders of magnitude. Since there is no single celestial source available to cover the broad energy range, the calibration of the LETGS effective area has been achieved in multiple phases: 1) the low energy study covering energies 0.06−0.28 keV (44−200 Å); 2) the mid-range study covering energies 0.28−2.0 keV (6−44 Å); and once those two were accomplished, 3) an implementation of the QE uniformity and derivation of a better HRC-S on-axis QE.

The low energy calibration of the LETGS was achieved by observing nearby hot white dwarfs (detailed in Pease et al. 2000a). White dwarfs with effective temperatures greater than 20000 K and photospheres composed of pure hydrogen should produce featureless continua in the LETG range. Furthermore, their photospheric models are considered to be fairly well understood. The white dwarfs employed for low energy calibration were Sirius B and HZ 43, whose X-ray flux levels useful for calibration covered $E < 0.21$ keV ($\lambda > 60$ Å).

The mid-range LETGS calibration (0.15−2.0 keV; 6−80 Å) was presented in preliminary form by Pease et al. (2000b; LETGS effective area version date 10/31/00). For this study we used data from observations of the blazar PKS 2155−304 and the quasar 3C 273, which both appear broadly to be featureless continua sources. The flux as a function of energy for these sources can be described by power-law models ($N \sim E^{-\Gamma}$). PKS 2155−304 (e.g. Treves et al. 1989; Urry et al. 1986), modeled by a single power-law, has been adopted as the primary calibration source. It covers the full mid-range energies of interest and the contribution from LETG higher orders is $\lesssim 10\%$ for $E > 0.25$ keV ($\lambda < 50$ Å), except at the C-K edge. The more complex spectrum of 3C 273 (e.g. Turner et al. 1985) requires a two power-law model, and its greater LETG high order contribution adds to this complexity. Therefore, 3C 273 has been used as a secondary and confirmatory source.

Though these sources are treated as essentially featureless continua, it is noted that with the high resolution X-ray spectra captured by the *Chandra* Low and High Energy Transmission Gratings (LETG and HETG) in combination with the High Resolution Camera (HRC) and the Advanced CCD Imaging Spectrometer (ACIS) spectral lines are certainly being found. From *Chandra* LETG/HRC-S observations of PKS 2155−304, Nicastro et al. (2002) found oxygen and neon resonant absorption lines associated with a warm-hot intergalactic medium. Meanwhile, Fang et al. (2002) analyzed *Chandra* LETG/ACIS observations and also report on an oxygen absorption line along the line of sight to PKS 2155−304. Thus, in order to avoid biasing the LETGS calibration, we have removed the data over energies for which lines and features inherent to the observed source spectra have been reported.

The final phase of the current LETGS effective area calibration (version date 07/02) was accomplished with the implementation of HRC-S QE uniformity and the fine-tuning of instrumental edge features, such as the C-K edge at ~ 0.28 keV (44 Å) and the Cs-M$_{iv,v}$ edges at ~ 0.74 keV (16.8 Å). These adjustments were made with a combination of synchrotron data obtained in the laboratory (Rideout et al. 1998) and in-flight observations. Particularly useful astrophysical sources for calibrating these instrument features were PKS 2155−304 and RX J1856.5−3754 (a compact object with a featureless apparently blackbody spectrum peaking near the C-K edge; e.g. Drake et al. 2002). For both sources we have obtained high signal-to-noise data sets covering instrument edge regions of interest.

This paper presents the calibration of the LETGS effective area and the HRC-S QE over the entire LETG active range. In §2 we present the observations and discuss data reductions, including background subtraction and spectral extraction; in §3 we derive an update to the effective area via the calibration of the HRC-S QE, rebuild the LETGS effective area, then derive and implement the HRC-S QE uniformity; and in §4 we discuss caveats and further work towards a more complete calibration of the LETGS effective area.

2. OBSERVATIONS AND DATA REDUCTION

The observations employed for the in-flight LETGS effective area calibration are summarized in Table 1. All data were pipeline-processed by CXC software to generate photon event lists. Data were further reduced and analyzed using the CIAO software package version 2.2 and independent custom IDL* software. Processing included extra pulse-height filtering to reduce background (Wargelin et al. 2002, in preparation), and inclusion of the spectral extraction efficiency in the instrument response.

The background rate in the HRC-S is much higher than pre-flight expectations due to a timing error in the implementation of its anti-coincidence shield. The rate is about 7×10^{-5} counts s^{-1} arcsec^{-2}, or 0.12 counts per pixel in 10^5 seconds. A dispersed line in the LETGS has a FWHM of ~ 7 pixels and stretches along the cross-dispersion direction by 20−65 pixels (as it goes from shorter to longer wavelengths, due to the LETG astigmatism). Therefore, $\approx 15−55$ background counts are expected in a 10^5 second exposure. In our filtering scheme we apply the "light filter" which reduces background by 50-70%, while removing $< 1\%$ of source X-rays.

---

*Interactive Data Language, Research Systems Inc.

Table 1. Summary LETG+HRC-S Calibration Observations

Target	Obs ID	Date	Exposure (s)	Status[a]
Sirius B	1452	1999-10-26	27527	primary
	1459	1999-10-27	11909	primary
	1421	1999-10-28	24706	primary
HZ 43	59	1999-11-12	39798	secondary
	1011	2001-05-18	18653	secondary
	1012	2001-08-18	19947	secondary
	2584	2002-01-01	19003	secondary
PKS 2155−304	331	1999-12-25	62658	primary
	1704	2000-05-31	25835	secondary
	1013	2001-04-06	26643	secondary
	3166	2001-11-30	29771	secondary
3C 273	460	2000-01-09	39939	secondary
RX J1856.5−3754	113	2000-03-10	55121	secondary
	3382	2001-10-08	101172	secondary
	3380	2001-10-10	166325	secondary
	3381	2001-10-12	169956	secondary
	3399	2001-10-15	9282	secondary

[a] Status column indicates whether observation was employed to make the semi-empirical corrections to HRC-S QE (primary) or to monitor/fine-tune the effective area (secondary)

Dispersed photon events were extracted using the standard "bow-tie" window, developed to follow the astigmatic nature of the LETG and optimize the signal-to-noise of the spectral extractions. The extraction efficiency varies from roughly 90% near zeroth order to more than 96% at the longest wavelengths. This extraction region efficiency is included in the final version of the LETGS effective area presented here.

3. EFFECTIVE AREA AND QUANTUM EFFICIENCY ANALYSIS

The LETGS effective area resulting from the low energy calibration and the preliminary mid-range adjustment (version date 12/15/01; Pease et al. 2000a and Pease et al. 2000b) has been the working effective area and represents a good first cut, with broadband errors of less than 20%, and much less on smaller scales. However, a comparison of our model-predicted counts spectrum for PKS 2155−304 with the LETGS observation ObsID 331, clearly shows residual errors (see Figure 1). We have broken the current calibration down into four bands: first, a higher energy mismatch over $\sim 1 - 6$ keV (2−12 Å) which arose from differences in extraction methods; second, Cs-$M_{iv,v}$ edges near ~ 0.74 keV (16.8 Å) which were inadequately included in the original pre-flight model; third, a misalignment of the C-K edge ~ 0.28 keV (44 Å) by about 0.3 eV; and fourth, a mid-to-low mismatch over $\sim 0.18 - 0.15$ keV (70−80 Å) which resulted, in part, from difficulties in matching the low energy calibration with the mid-range study. In addition to resolving the above issues, an HRC-S QE uniformity map was derived and implemented.

In order to correct the LETGS effective area we assumed that the residuals of the data-to-model comparisons were errors in the HRC-S QE model. Thus, a correction to the HRC-S QE was derived such that the predicted and observed spectra match. The effective area then depends implicitly on the adopted source models. This method, while simple in concept, is complex in implementation due to the source model dependence. Furthermore, the LETG positive and negative dispersions were calibrated separately, due to the complex nature of the HRC-S QE uniformity.

The white dwarf emission models used for the low energy calibration were previously presented and discussed by Pease et al. (2000a). For the subsequent mid-range calibration and further fine-tuning of the LETGS
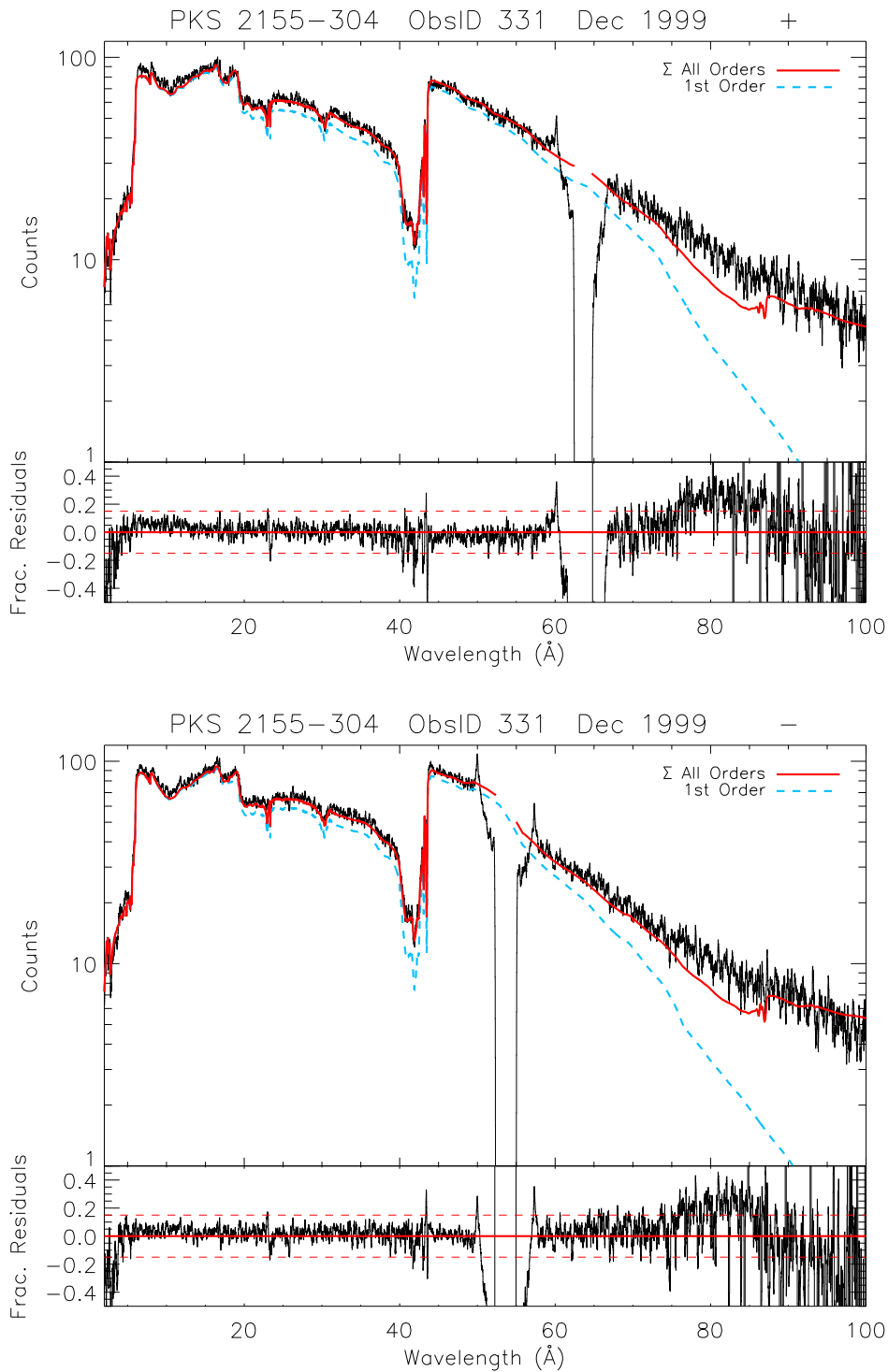
Figure 1. Comparison of the pre-correction model-predicted spectrum for PKS 2155−304 with the observed LETGS spectrum (ObsID 331) illustrates inadequacies in the model (see large fluctuations in the residuals), which we attribute to errors in the HRC-S QE. Dashed lines on residuals plots are 15% error lines. Positive and negative orders are plotted separately. Data have been smoothed by 10 pixels (1 pixel = 0.0125 Å).

effective area, PKS 2155−304, 3C 273, and RX J1856.5−3754 were the sources of choice. Power-law models for PKS 2155−304 and 3C 273 have been defined from HETG/ACIS observations, for which we were able to derive a reliable spectral index at the high energy end. For the primary calibration observation of PKS 2155−304 (ObsID 331) we adopted a single power law with $\Gamma = 2.45$, and Galactic hydrogen column density of $N_{\rm H} = 1.36 \times 10^{20}$ cm^{-2} ($N_{\rm H}$ from Lockman and Savage 1995). 3C 273 (ObsID 460) was modeled by a two power law model with $\Gamma_1 = 1.56$, $\Gamma_2 = 2.1$, with a break at ~ 0.8 keV (15.5 Å), and $N_{\rm H} = 1.71 \times 10^{20}$ cm^{-2} ($N_{\rm H}$ from Albert et al. 1993). Finally, the X-ray spectrum of the compact object RX J1856.5−3754 was well-represented by an ~ 60 eV (7×10^5 K) blackbody, with an interstellar medium neutral hydrogen column density of 8×10^{19} cm$^{-2} \leq N_{\rm H} \leq 1.1 \times 10^{20}$ cm^{-2} (Drake et al. 2002).

The high energy mismatch and the Cs-M edges issue were resolved by the correction method described above, using primarily PKS 2155−304. The Cs-M edges correction also employed data and analysis from Rideout et al. (1998). While their synchrotron data clearly did not match the observed LETGS data[†], we did use it as a guide to the general edge shape. These two corrections were produced by highly constrained, smoothed spline fits to the residuals of the ratio of the observed data to the initial model. Next, the correction to the mid-to-low mismatch was achieved simply by smoothing an interpolation over the joining region in the HRC-S MCP QE. This correction is small compared to the adjustment necessary to match the model to the PKS 2155−304 data. We find that the gross residual at the longer wavelength end can be attributed to inadequacy of the PKS 2155−304 source model, not the LETGS effective area. The correction curves are shown in Figure 2.
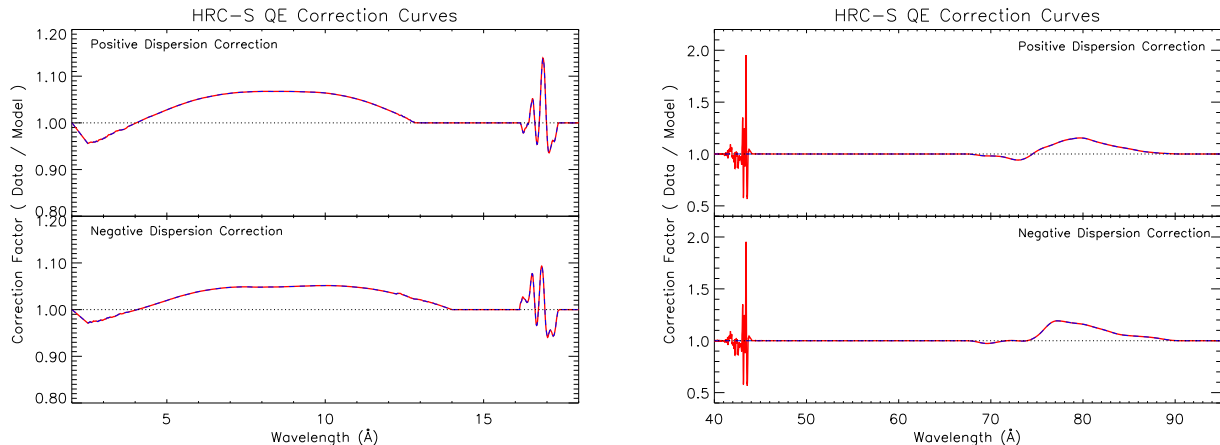

Figure 2. HRC-S QE fine-tuning correction curves derived from in-flight calibration using primarily PKS 2155−304 (ObsID 331). The left plot shows corrections to the high energy mismatch and the Cs-M edges. The right plot shows the HRC-S UV/ion shield shift and the smoothing of the MCP QE mid-to-low calibration joining region. Positive and negative dispersion corrections are shown separately.

The instrumental C-K edge feature is due to carbon in the HRC-S UV/ion shield. The observed edge mismatch is likely due to error in the energy calibration of the synchrotron measurements used to calibrate the UV/ion shield transmission efficiency[‡]. To correct the C-K edge we simply applied a -0.25 eV linear shift to the UV/ion shield transmission efficiency model over the range of 0.28−0.3 keV (41−44 Å). This brought the primary edge jump and most of the fine-structure resonance peaks into alignment with the observed data. However, there remains some residual mismatch near $\sim$0.288 keV (43 Å). We suspect this feature comes from insufficiently modeled resonance fine structure. A correction will be implemented after further study that includes the effects of the relationship between the carbon in the UV/ion shield and that in the ISM. The C-K edge correction is included in the correction curves shown in Figure 2.

[†]For discussion of the ALS wavelength error observed at BESSY see Flanagan et al. (2000)

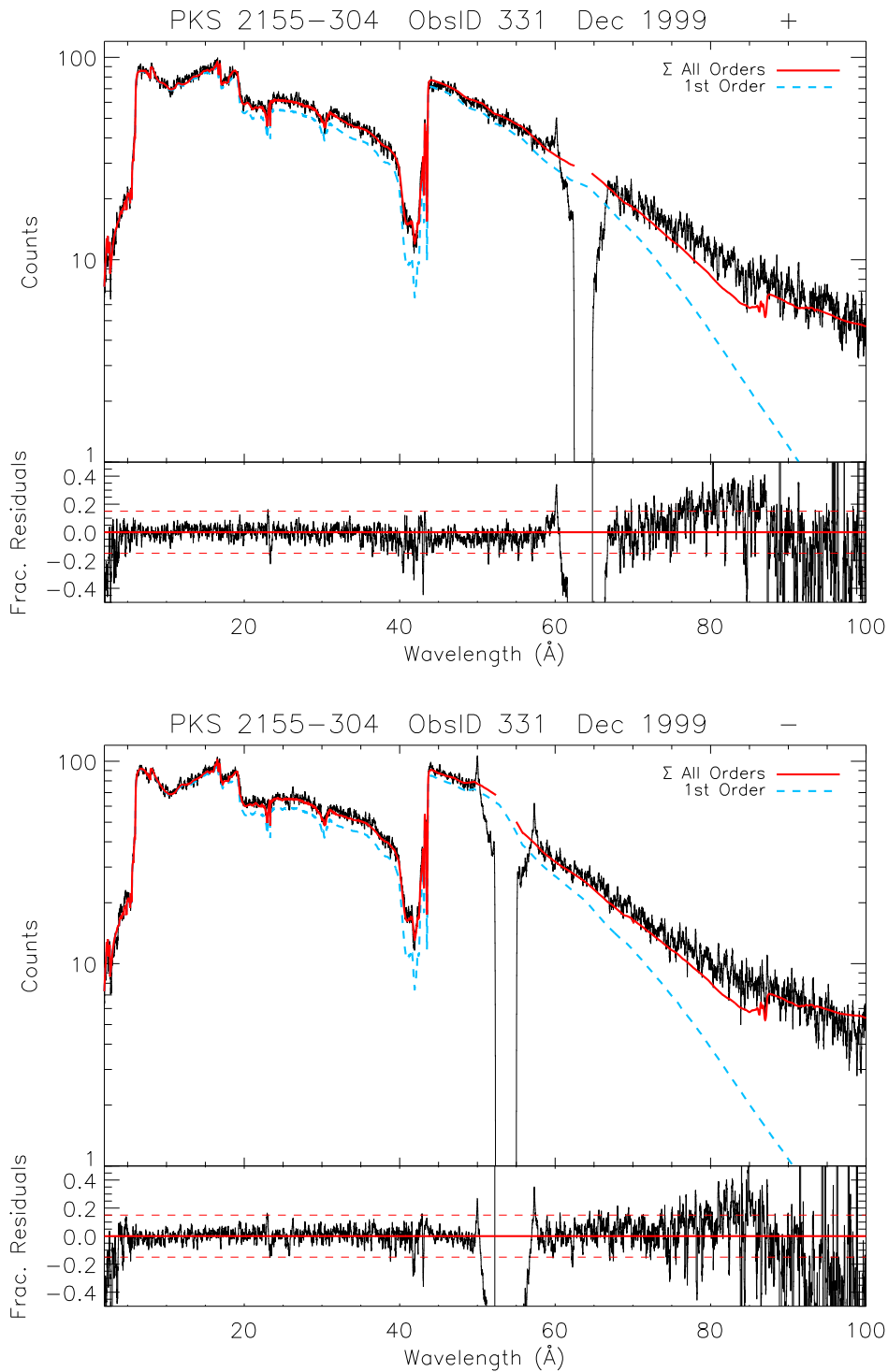[‡]See HLM's webpage: http://space.mit.edu/ASC/calib/letg_acis/

Figure 3. Comparison of the new post-correction model spectrum, employing the improved LETGS effective area, with the observed spectrum for PKS 2155−304 (ObsID 331). The remaining residual at long wavelengths is due to the inadequacy of a single power law source model. Dashed lines on residuals plots are 15% error lines. Positive and negative dispersions are shown separately. Data have been smoothed by 10 pixels (1 pixel = 0.0125 Å).

Applying the correction curves described above to the HRC-S QE model, we rebuilt the semi-empirically determined LETGS effective area, and the re-computed model spectra to compare with the data (Figure 3). Details of this comparison over the energy regimes of interest are shown in Figure 4. As expected, the residuals are well behaved. We further compare the post-correction LETGS response with 3 independent observations of PKS 2155−304 (ObsIDs 1704, 1013, 3166) and an observation of 3C 273 (ObsID 460) (Figures 5−8). We see generally good agreement with all observations.

The next step was to derive a model for the HRC-S QE uniformity. Prior to launch, flatfield data were acquired in the laboratory at 7 energies which ranged from 0.18 keV to 6.4 keV. From these an energy-dependent spatial model of the HRC-S QE was derived. To illustrate the spatial structure of the HRC-S QE along the dispersion axis, Figure 9 shows the derived QEU for a rectangular strip located within the nominal extraction region of the LETG. This line is representative of a transection of the QEU, for which wavelength is paired with LETG dispersion location unique to photon energy. By applying this QEU model to the semi-empirically determined LETGS effective area, we removed the effects of dispersion and derived a better HRC-S on-axis QE. To illustrate the dramatic effect of the QEU along the LETG dispersion line, Figure 10 shows the new, post-correction on-axis MCP QE plotted with the MCP QE curves for the positive and negative dispersions of the LETG. Thus, the implementation of the HRC-S QEU with the new on-axis QE now allows for the computation of effective area for any reasonable *Chandra*/LETGS pointing.

Finally, in Figure 11 we show the LETGS effective area curves for orders 0−3 with positive and negative orders combined.

4. PHILOSOPHY, UNCERTAINTIES, AND FUTURE WORK

Our philosophy for executing the in-flight LETGS calibration has been to make the necessary adjustments without making radical changes which may be difficult to disentangle in future updates. Thus, the corrections to the HRC-S QE outside of edge regions are kept as smooth as possible to avoid introducing spurious features[§]. Using this method, as calibration monitoring continues, persistent small scale mismatches can be easily discerned and investigated for possible inclusion in the model, without getting obscured by previous model corrections.

A rigorous quantification of the uncertainties in the LETGS effective area derived here would involve a highly complicated error analysis. Each of the ingredients in the effective area has associated uncertainties, but these ingredients are mixed in ways which make do not lend themselves easily to such analysis.

Prior to launch, the total effective area uncertainties could be described in gross terms by combining the uncertainties of the different LETGS subassemblies: High Resolution Mirror Assembly (HRMA) effective area, LETG vignetting and diffraction efficiencies, HRC-S UV/ion shield transmission efficiency, and HRC-S QE. Following calibration activities at the Marshall Space Flight Center X-ray Calibration Facility (XRCF; e.g. Weisskopf and O'Dell 1997), the uncertainties in all of these subassembly calibrations, except for the HRC-S QE, were known to be "small"— $\lesssim 10\%$ for 1st order diffraction (Drake et al., in preparation). Largely due to modifications to the HRC-S instrument that were made post-XRCF, uncertainties in its QE were much larger, and it was essentially undetermined at low energies (< 0.25 keV; $\lambda > 50$ Å; Pease et al. 2001a). Consequently, as we have described in this paper, in-flight calibration activities have concentrated on determining this QE, with the assumption that existing calibrations of the other subassemblies are correct.

The in-flight calibration, in contrast, examines the throughput of the LETGS as a whole (including higher orders); implicit in this method, then, is that true errors in the calibrations of the other subassemblies will be subsumed and compensated for by commensurate errors of opposite sign induced in the empirically-adjusted QE. If the 1st order diffraction could be treated in isolation for on-axis pointing, the empirically-adjusted 1st order effective area would then simply be as accurate as our source models for the celestial objects upon which the calibration is based. We have estimated that the source models typically have absolute flux level uncertainties of $10-15\%$ (Drake et al., in preparation). Relative uncertainties on small scales are much smaller than this,

---

[§]For example, it appears that PKS 2155−304 is not best described by a single power law. In fact we have shown evidence that at least a double power-law model may be required (Figure 3). In the future, we anticipate that the single power law will be replaced by a better model for the broad shape of the response.

except near significant instrument edge features. Such relative errors are expected to grow over wavelength ranges (typically ~ 50 Å) spanned by individual celestial calibration sources.

The main issue that complicates this description of the 1st order effective area calibration uncertainty is higher order diffraction. For this calibration we have accounted for all available modeled LETG diffraction efficiencies ($\sum O\ 1 - 25$) in deriving and fine-tuning the effective area. Because of the lack of energy resolution of the HRC-S, these spectral orders are inseparable. Thus, in analogy with the discussion above regarding errors in the calibrations of the different subassemblies, errors in higher order diffraction efficiencies will likewise be subsumed into the HRC-S QE. However, the errors thus induced in the QE no longer directly compensate each other because the errors are induced at different wavelengths to the wavelengths of the diffraction efficiency errors; an error in diffraction efficiency of order m at wavelength λ will affect the QE at wavelength $m\lambda$.

In the wavelength regime in which our QE calibration is based wholly on DA white dwarfs (> 80 Å), higher order diffraction is negligible because it tends to be dispersed to distances beyond the end of the HRC-S array, and because the source spectra are weak at short wavelengths. We can then be reasonably confident that for > 80 Å, the absolute error in the 1st order effective area is of order $10-15\%$. Similar arguments hold for the shortest wavelengths: throughout the range $\sim 2-20$ Å the higher order contribution to the total observed counts amounts to $\lesssim 5\%$, and again the errors in the effective area will be of order $10-15\%$. The complications arise in the intermediate wavelength regime.

Currently under investigation is evidence suggesting that the model diffraction efficiencies for orders 2 and 3 might be overestimated by as much as $30-40\%$ for energies < 0.5 keV (> 25 Å). Such errors would impact the QE at E/m or $m\lambda$—the region of the C-K edge down to the regime where DA white dwarfs are exclusively used. Where 1st order dominates the PKS $2155-304$ spectrum, such as near the C-K edge, these errors are relatively minor. The largest uncertainties in our effective area calibration will be in the approximate energy range $0.15-0.2$ keV ($60-80$ Å), where we expect uncertainties might be as large as $20-25$ %.

As we have described, the LETGS calibration is reliant on cross-calibration among various instrument configurations. To date, we have employed *Chandra* observations with HETG/ACIS and LETG/ACIS to obtain adequate models for LETG/HRC-S data sets. ACIS grating data are considered simpler to work with because order separation is feasible using the pulse height discrimination of the ACIS instrument. However, some uncertainty inherent in using these data comes from the fact that they only overlap with LETG/HRC-S at higher energies. In addition, the ACIS-S instrument also has intrinsic absolute QE uncertainties of order $\sim 10\%$. Ongoing cross-calibration activities with *XMM-Newton* should yield new insights in this regard. Simultaneous observations of PKS $2155-304$ (in addition to 3C 273 and Capella) have been performed and are now part of routine calibration activities of both satellites. In particular, joint cross-calibration efforts will help resolve uncertainties in the source model for PKS $2155-304$ upon which much of our current in-flight calibration activity rests.

REFERENCES

1. Albert, C. E. et al. 1993, ApJS, 88, 81
2. Brinkman, A. C. et al. 2000a, ApJ, 530, L111
3. Brinkman, B. C. et al. 2000b, Proc. SPIE, 4012, 81
4. Drake, J. J. et al. 2002, ApJ, 572, 996
5. Fang, T. et al. 2002, ApJ, 572, L127
6. Flanagan, K. A. et al. 2000, Proc. SPIE, 4140, 559
7. Lockman, F. J. & Savage, B. D. 1995, ApJS, 97, 1
8. Nicastro, F. et al. 2002, ApJ, 573, 157
9. Pease, D. et al. 2000a, Proc. SPIE, 4012, 700
10. Pease, D. et al. 2000b, BAAS/High Energy Astrophysics Division, 32, 43.05
11. Rideout, R. M. et al. 1998, Proc. SPIE, 3445, 384
12. Treves, A. et al. 1989, ApJ, 341, 733
13. Turner, M. J. L. et al. 1985, Space Science Reviews, 40, 623
14. Urry, C. M., Mushotzky, R. F., & Holt, S. S. 1986, ApJ, 305, 369
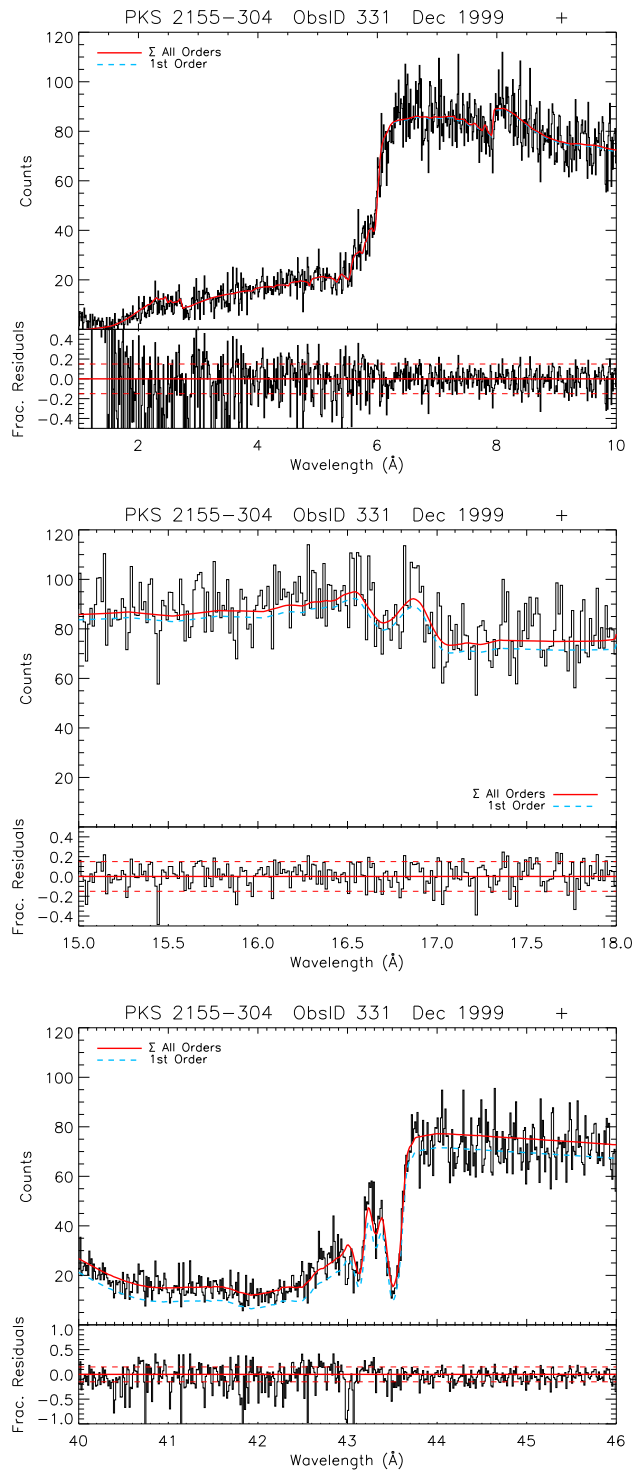15. Weisskopf, M. C. & O'Dell, S. L. 1997, Proc. SPIE, 3113, 2

Figure 4. Details of the energy regimes of interest. The top plot shows the repaired higher energy mismatch over $\sim 1-6$ keV ($2-12$ Å). The middle plot shows the inclusion of the Cs-M$_{iv,v}$ edges near ~ 0.74 keV (16.8 Å). The bottom plot shows the improved alignment of the C-K edge ~ 0.28 keV (44 Å). Note the remaining mismatch at ~ 43 Å. Dashed lines on residuals plots are 15% error lines. Data have been binned by CIAO pixel size (0.0125 Å). Only data from positive dispersion are shown. Negative dispersion corrections display similar results.
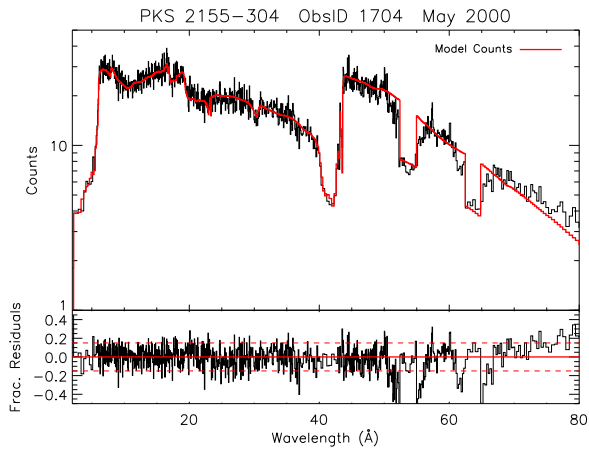
Figure 5. Post-correction model prediction compared with the May 2000 observation of PKS 2155−304, $\Gamma = 2.42$. Positive and negative orders have been combined and the spectrum has been adaptively binned to signal-to-noise of 7.5. Dashed lines on residuals plots are 15% error lines. Modeled gaps do not include the effects of dither.
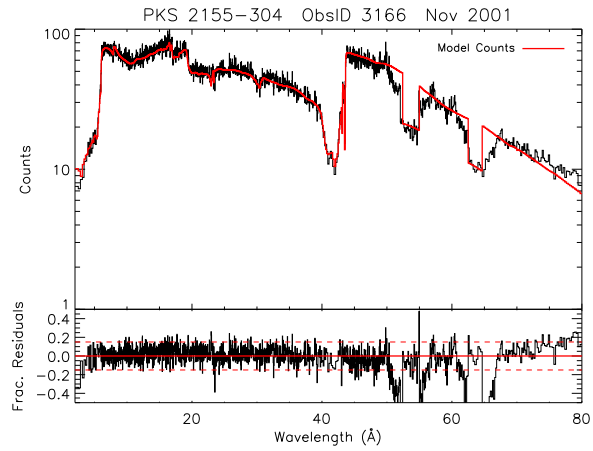

Figure 7. As for Figure 5, post-correction model prediction compared with the November 2001 observation of PKS 2155−304, $\Gamma = 2.45$.
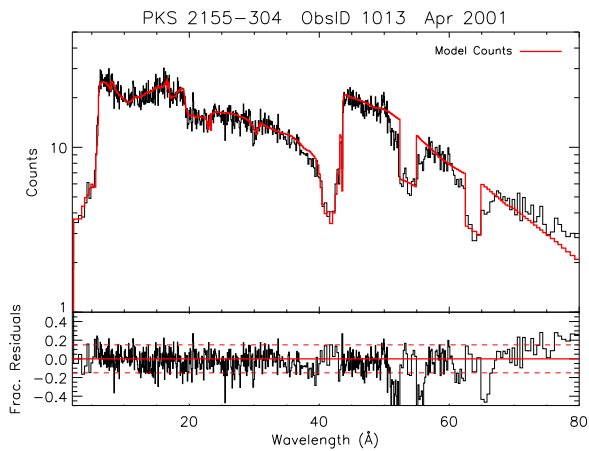
Figure 6. As for Figure 5, post-correction model prediction compared with the April 2001 observation of PKS 2155−304, $\Gamma = 2.38$.
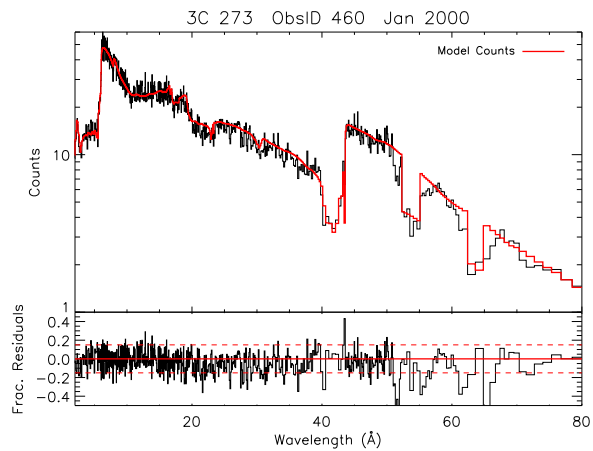

Figure 8. As for Figure 5, post-correction model prediction compared with the January 2000 observation of 3C 273, $\Gamma_1 = 1.56$, $\Gamma_2 = 2.1$, an independent source to confirm the calibration.
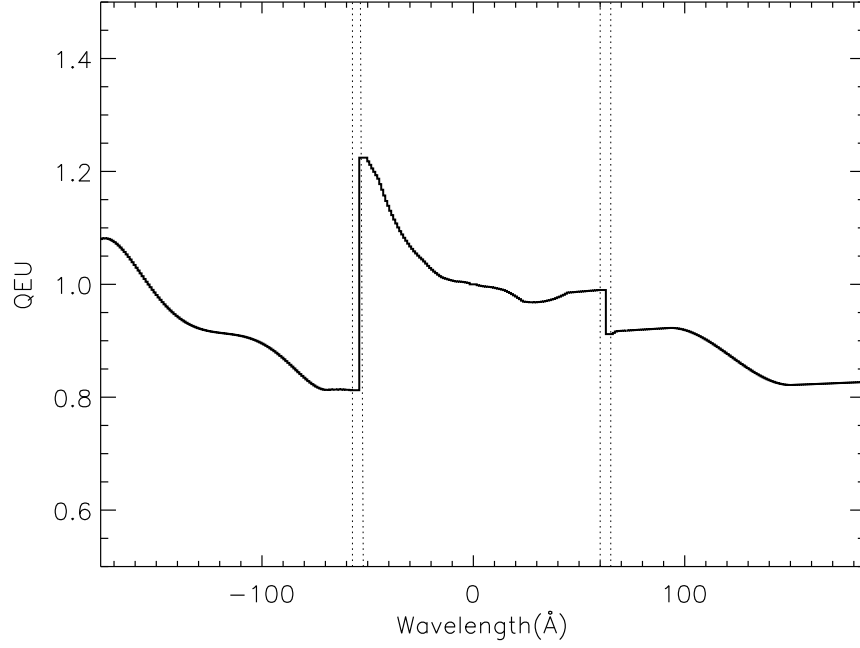
Figure 9. The HRC-S QE uniformity curve for a rectangular strip located within the LETG nominal extraction region. Wavelength is paired with LETG dispersion location unique to photon energy. The vertical dotted lines indicate plate boundaries.
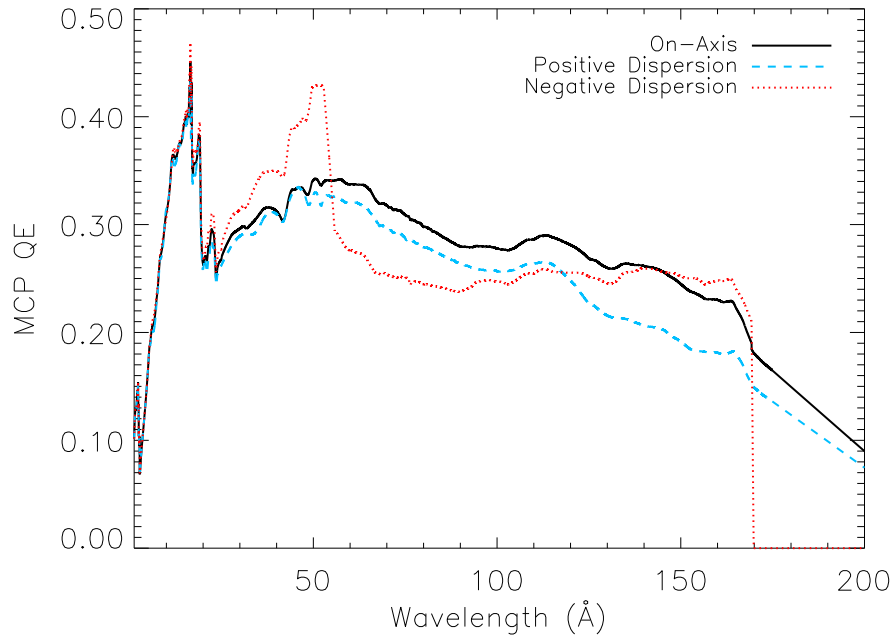

Figure 10. The new, post-correction on-axis MCP QE shown along with the MCP QEs which follow positive and negative LETG dispersions. This figure also serves to illustrate the effects of the non-uniformity of the MCP QE.
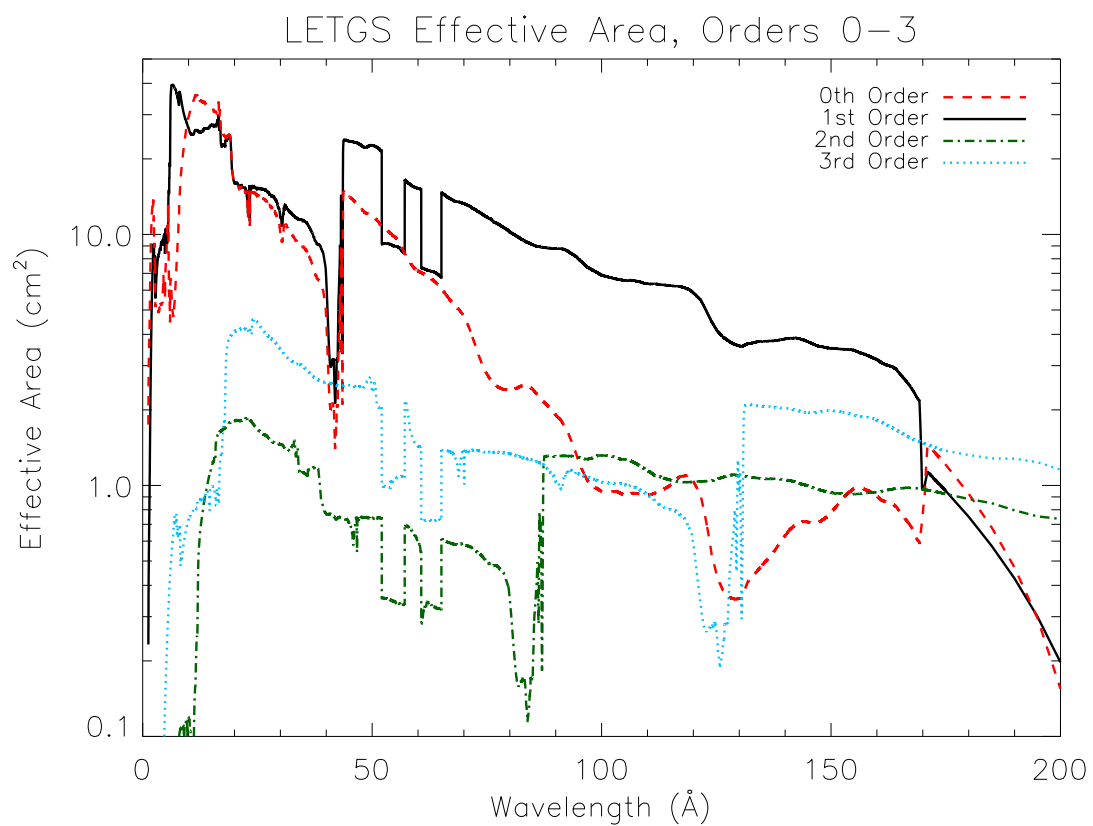
Figure 11. The LETGS effective area curves for 0th, 1st, 2nd, and 3rd orders of dispersion. Higher order effective areas are plotted along the 1st order scale. Positive and negative orders have been combined.